Title

Numerical Study of Deformation Behavior of Geosynthetic Reinforced Soil Bridge Abutments Subjected to Longitudinal Shaking

ISBN

9783030772338

Authors

Zheng, Yewei
Fox, Patrick J
McCartney, John S

Publication Date

2022

DOI

10.1007/978-3-030-77234-5_41

Peer reviewed

Numerical study of deformation behavior of geosynthetic reinforced soil bridge abutments subjected to longitudinal shaking

Yewei Zheng[1][0000-0001-9038-4113], Patrick J. Fox[2][0000-0001-7279-3490], and John S. McCartney[3][0000-0003-2109-0378]

[1] Professor, School of Civil Engineering, Wuhan University, Wuhan, Hubei, 430072 China; yzheng@whu.edu.cn

[2] Shaw Professor and Head, Department of Civil and Environmental Engineering, Pennsylvania State University, University Park, PA 16802, USA; pjfox@engr.psu.edu

[3] Professor and Chair, Department of Structural Engineering, University of California San Diego, La Jolla, CA, 92093-0085, USA; mccartney@ucsd.edu

Abstract. This paper presents a numerical study on the deformation behavior of geosynthetic reinforced soil (GRS) bridge abutments subjected to longitudinal shaking using the finite difference program FLAC. The soil model characterizes the soil as an elastic-plastic material with hysteretic behavior. Numerical simulations were conducted for a single-span full bridge system, including the bridge beam, two GRS abutments, and foundation soil, subjected to the 1940 Imperial Valley motion in the longitudinal direction. Simulation results show that the two front wall facings in each abutment moved in-phase during shaking and had different residual facing displacements at the end of shaking due to asymmetry of the earthquake motion with respect to the abutment geometry. Bridge seat settlements at the two ends of the bridge system were similar.

Keywords: Geosynthetic reinforced soils, Bridge abutment, Earthquake.

1 Introduction

Geosynthetic reinforced soil (GRS) bridge abutments are becoming widely used for transportation infrastructure in the United States. Although this technology offers substantial cost- and time-savings for construction, there are concerns regarding the use of GRS bridge abutments technology in high seismic areas and little information is available to guide designers on how to improve the seismic performance of these structures.

Post-earthquake reconnaissance for the 2010 Maule earthquake and found that a GRS abutment exhibited no signs of lateral or vertical permanent displacements after shaking, while the bridge suffered minor damage that may have resulted from the bridge skew angle [1]. Shaking table tests have been conducted on GRS abutments

for shaking in the longitudinal direction to the bridge beam [2, 3, 4]. Shaking table tests on a 3.6 m-high GRS abutment indicated no significant distress for longitudinal shaking with horizontal accelerations up to 1g [2]. Results from a series of shaking table tests on 2.7 m-high half-scale GRS abutments subjected to scaled earthquake motions indicated that residual facing displacements and bridge seat settlements increased with larger reinforcement vertical spacing, reduced reinforcement stiffness, and lower surcharge stress under dynamic loading [3, 4].

Although these studies indicate good overall performance for GRS abutments under dynamic loading, the abutments specimens were limited by the size and payload capacity of the shaking table. Numerical modeling can be used to investigate potential seismic issues for GRS abutments with more realistic geometry and configuration. In this study, the two-dimensional finite difference program FLAC was used to simulate the deformation behavior of a single-span full bridge system using two GRS abutments for earthquake shaking in the longitudinal direction.

2 Numerical Model

2.1 Model Configuration

The single-span full bridge system investigated in this study consists of a bridge beam and two GRS abutments. Model geometry for the right-hand side of the bridge system is shown in Fig. 1 for simplicity, and the left-hand side is symmetric. The bridge system has a span L_b = 30 m and symmetrical structures on both ends, resting on foundation soil with a depth of 1 m. Each end structure consists of a lower GRS wall, bridge seat, and upper GRS wall. The lower GRS wall has height h = 5 m and 25 modular facing blocks with dimensions of 0.3 m (length) × 0.2 m (height). An L-shaped bridge seat with a vertical backwall rests on top of the lower GRS wall and has setback distance a_b = 0.2 m from the wall facing. The clear distance between the top facing block and bridge beam d_e is equal to the bridge seat thickness (0.4 m). The clearance height for the bridge beam above the foundation soil is 5.4 m, which satisfies the FHWA minimum requirement of 4.9 m for interstate highways [5]. The bridge seat has upper surface contact length L_c = 1.0 m with the bridge beam and lower surface contact length L_s = 1.5 m with the backfill soil. There is a 100 mm-wide vertical seismic joint between the bridge beam and the backwall of bridge seat. Assuming a ratio of bridge beam span to depth $R_{sd} = L_b/D$ = 20, the depth of the bridge beam D = 1.5 m. A 1.9 m-high upper GRS wall lies behind the backwall of bridge seat. To minimize the influence of boundary conditions on system response, the lateral boundaries are located at a distance of 30 m (6h) from the front wall facing on each end of the bridge. The vertical coordinate z is measured upward from the top surface of the foundation soil.

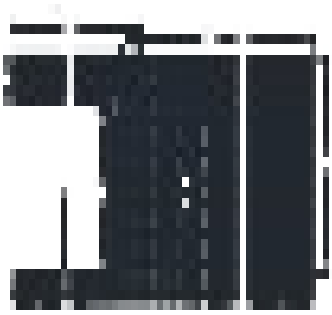

Fig. 1. Model geometry for the right-hand side of bridge system (left-hand side symmetric).

2.2 Material Model and Properties

Soils

The soil properties for this study are characterized of a well-graded sand. The angular sand has a high friction angle of 51.3° and zero cohesion according to results from drained triaxial compression tests on dry sand specimens. The foundation soil was assumed to be the same with the backfill soil and represented a dense sand foundation. For static analysis, the backfill soil and foundation soil were modeled as a nonlinear elastic-plastic material using the Duncan-Chang hyperbolic relationship [6] and the Mohr-Coulomb failure criterion. This model can capture the nonlinear stress-strain behavior before the peak shear strength and dilation behavior. Details of the soil model are reported by Zheng and Fox [7, 8].

For dynamic analysis, the UBCHYST model [9] was used in this study. This model can account for reduction in secant modulus with increasing shear strain. The tangent shear modulus is a function of the small strain shear modulus G_{max} times a reduction factor that is a function of the developed stress ratio and change in stress ratio to reach failure. In this study, the small strain shear modulus G_{max} is estimated using the empirical relationship proposed by Menq [10]. The model parameters, as summarized in Table 1, were calibrated by comparing cyclic simple shear response to the modulus reduction curves and damping curves calculated using published empirical relationships [10, 11]. The shear stress-strain relationships from the numerical simulations for different mean effective stresses and cyclic shear strain amplitudes are shown in Fig. 1**.** The model exhibits hysteretic soil behavior that is consistent with that observed for sands [10].

Table 1. UBCHYST model parameters.

Parameter	Value
Friction angle, ϕ' (°)	51.3
Cohesion, c' (kPa)	0
Small strain shear modulus, G_{max} (MPa)	Stress-dependent
Bulk modulus, B (MPa)	= G_{max}
Atmospheric pressure, p_a (kPa)	101.3
Hysteretic parameter, H_n	6.0
Hysteretic parameter, H_{n1}	1.0
Hysteretic parameter, H_{rf}	0.98
Hysteretic parameter, H_{rm}	1.0
Hysteretic parameter, H_{dfac}	0

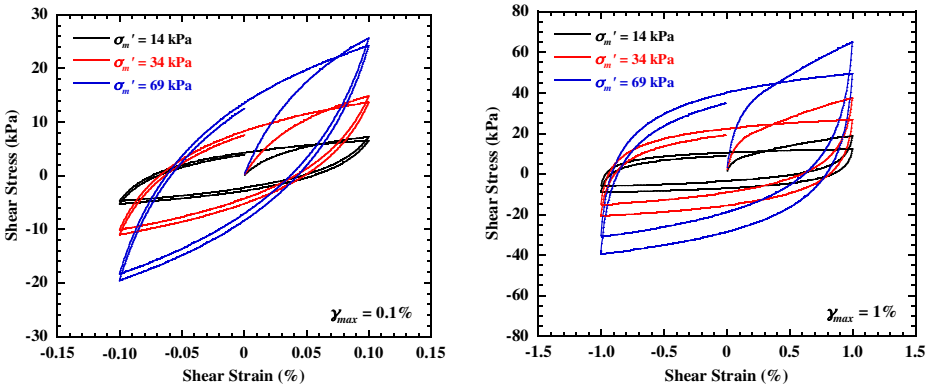

Fig. 1. Simulated shear stress vs. shear strain: (a) γ_{max} = 0.1%; (b) γ_{max} = 1%.

Reinforcements

The geogrid layers in both the lower and upper GRS walls had a uniform length L_r = 3.5 m (0.7h) and vertical spacing S_v = 0.2 m. No secondary (i.e., bearing bed) reinforcement layers were included under the bridge seat. The geogrid reinforcements were simulated using linearly elastic-plastic cable elements with tensile stiffness J = 1000 kN/m and yield tensile force T_y = 100 kN/m. The ultimate yield strength of 100 kN/m was selected as the yield tensile force for the geogrid.

Structural Components

The concrete facing blocks and bridge seat were modeled as elastic materials with unit weight γ = 23.5 kN/m^3, elastic modulus E = 20 GPa, and Poisson's ratio v = 0.2. A longitudinal slice of the bridge beam with unit width was modeled as a solid block composed of elastic elements having an equivalent unit weight γ_{eq} = 13.33 kN/m^3 to produce an average vertical stress of 200 kPa on the lower GRS wall.

Interfaces
Various interfaces between soil, geogrids, blocks, and structures were simulated using interface elements with Coulomb sliding behavior. The bearing pads between the bridge beam and bridge seats on each end were simulated using interface elements with a friction coefficient of 0.4 [12].

2.3 Modeling Procedures

For static analysis, prior to dynamic loading, the GRS abutments were constructed in stages with the bottom boundary fixed in both horizontal and vertical directions and the lateral boundaries fixed in the horizontal direction. Details of numerical modeling of GRS abutments under static loading are provided by Zheng and Fox [7, 8]. For dynamic analysis, free-field conditions were applied at the lateral boundaries of the model to absorb energy and prevent seismic waves from reflecting back into the problem domain. The earthquake motion was the 1940 Imperial Valley motion (El Centro Station). The acceleration time history is shown in Fig. 2, and yields a peak horizontal acceleration (PHA) of 0.31*g* and peak horizontal displacement (PHD) of 130.4 mm with a duration of 40 s. The earthquake motion was applied at the bottom boundary of the model in the longitudinal direction. In addition to the hysteretic stress-strain behavior, a small amount of Rayleigh damping (0.8%) was specified for the soil.

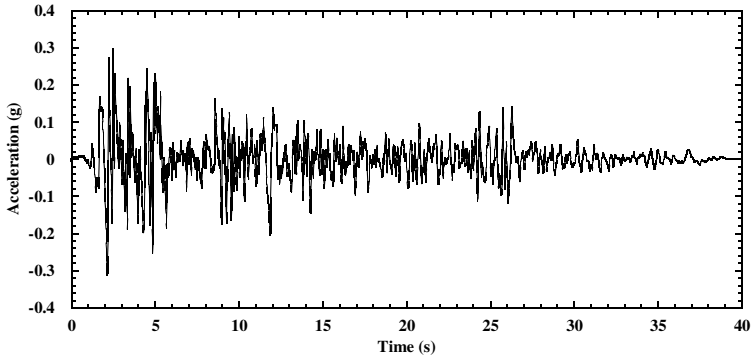

Fig. 2. Acceleration time history for the 1940 Imperial Valley motion (El Centro Station).

3 Simulation Results

This study focuses on the deformation behavior of a bridge system using two GRS abutments subjected to longitudinal shaking, and the reinforcement tensile strains and forces are not included in the discussion. The seismic performance of GRS abutments is evaluated in terms of incremental facing displacements, abutment vertical compression, and width of the vertical seismic joint (i.e., gap) between the bridge beam and the backwall of bridge seat. The incremental facing displacement is taken relative to the initial facing displacements at the end of construction (i.e., before the

start of shaking), with the outward displacements defined as positive. The abutment vertical compression is defined as the difference between the average bridge seat settlement and foundation soil settlement.

3.1 Facing Displacements

Time histories of incremental facing displacement at selected elevations for the left and right abutments are shown in Fig. 3. Each wall experienced larger facing displacements at higher elevations and permanent (i.e., residual) deformations by the end of the shaking. Results show that one facing moved outward when the other facing moved inward, which indicate the two wall facings moved approximately in-phase during shaking. Because the Imperial Valley earthquake motion shown in Figure 3 is not symmetric, when it is applied longitudinally to the bridge beam, the abutments will experience the opposite motions. The simulated facing displacements for the right abutment are larger than those for the left abutment because the applied motion causes greater accelerations in the direction of the wall face for the right abutment.

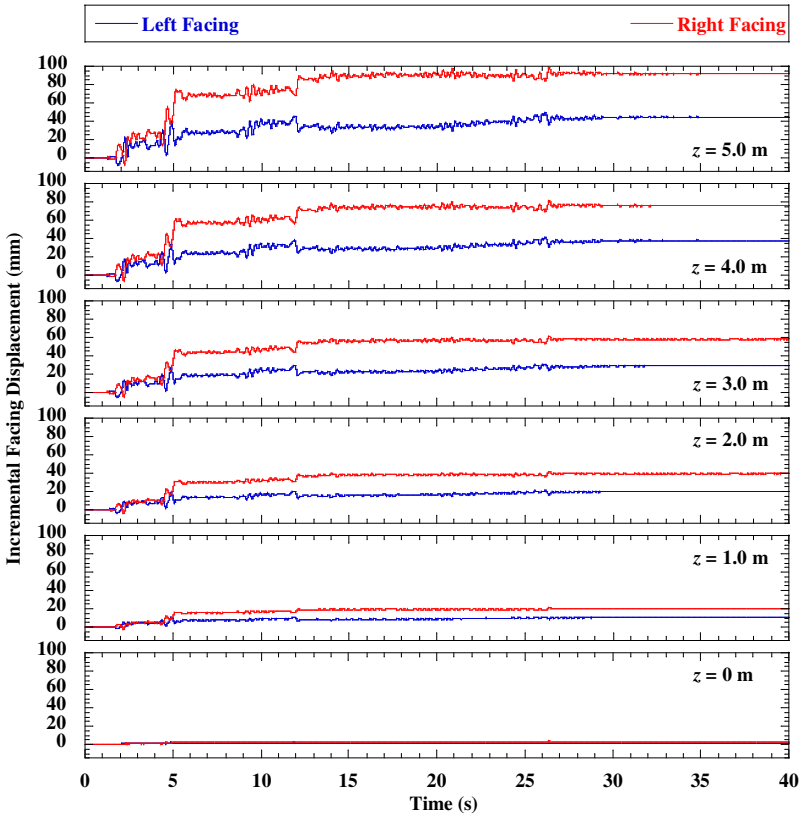

Fig. 3. Time histories of incremental facing displacements.

Profiles of incremental maximum and residual facing displacements are shown in Fig. 4. The profiles display similar shapes with incremental displacements increasing with elevation and highest values at the top of the walls. The maximum facing displacements for each wall are slightly larger than the residual displacements, which indicates that only a small amount of recovery at the end of shaking. The maximum residual facing displacements were 44.4 mm and 92.2 mm at the top of the wall for the left and right abutments, respectively.

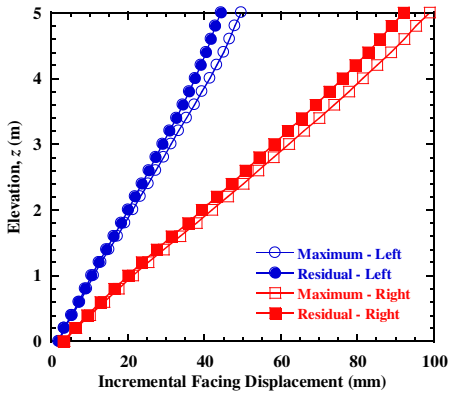

Fig. 4. Profiles of incremental facing displacements.

3.2 Abutment Vertical Compressions

Time histories of vertical compression for the left and right abutments are shown in Fig. 5, and indicate similar shapes with respect to both magnitudes and trends. The abutment compressions increased significantly to approximately 4 mm at t = 2 s and to approximately 9 mm at t = 5 s, and then remained nearly constant thereafter. The residual vertical compressions were 9.2 mm and 9.8 mm for the left and right abutments, respectively, corresponding to vertical strains of 0.18% and 0.20% for the 5 m-high lower GRS walls. These magnitudes of vertical strain are relatively small and would not be expected to cause significant damage to most bridge structures.

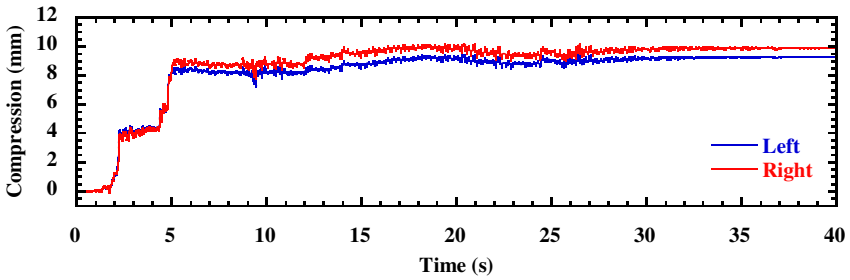

Fig. 5. Time histories of abutment vertical compression.

3.3 Seismic Joint Widths

During shaking, the bridge beam interacted with the GRS abutments through friction developed on the bearing pad interfaces, and the bridge beam may potentially contact the backwall of bridge seat when the seismic joint closes. Time histories of seismic joint width on each side of the abutment are shown in Fig. 6. The initial width of the seismic joints was 92.5 mm before the shaking event, and then decreased during shaking. Both seismic joints decreased in width because of the inward movement of the bridge abutments (i.e., toward the center of the bridge beam). The residual widths were 9.1 mm and 50.8 mm after shaking on the left and right sides of the bridge beam, respectively, which depended on the inward movement of the abutment and the horizontal displacement of the bridge beam. The inward movement of the abutment was different on either end of the bridge due to the asymmetric earthquake motion applied in the in the direction longitudinal to the bridge beam. Joint closure did not occur during shaking at either end of the bridge abutment, and thus no impact force occurred between the bridge beam and the backwall of bridge seat.

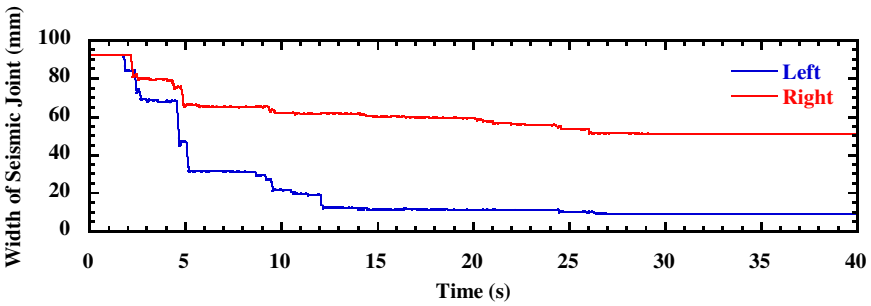

Fig. 6. Time histories of seismic joint width.

4 Conclusions

This paper presents a numerical study on the deformation behavior of geosynthetic reinforced soil (GRS) bridge abutments subjected to longitudinal shaking using the finite difference program FLAC. For the 1940 Imperial Valley motion in the

longitudinal direction, simulation results indicate that the two wall facings of the bridge system moved in-phase during shaking, but had different residual facing displacements at the end of shaking due the inward movement of the abutment and the horizontal displacement of the bridge beam. This occurred due to asymmetry of the earthquake motion in the direction longitudinal to the bridge beam. Abutment vertical compressions on the two ends of the bridge beam are similar and relatively small, which would not be expected to cause significant damage to most bridge structures. Vertical seismic joints between the bridge beam and the backwall of bridge seat decreased in width because of the inward movement of the two GRS abutments (i.e., toward the center of the bridge beam), but did not close for this earthquake motion.

References

1. Yen, W.-H.P., Chen, G., Buckle, I., Allen, T., Alzamora, D., Ger, J., and Arias, J.G. (2011). *Post-earthquake reconnaissance report on transportation infrastructure: Impact of the February 27, 2010, offshore Maule Earthquake in Chile*, FHWA-HRT-11-030, U.S. DOT, Washington, D.C.
2. Helwany, S.M.B., Wu, J.T.H., and Meinholz, P. (2012). *Seismic design of geosynthetic-reinforced soil bridge abutments with modular block facing.* NCHRP Web-Only Document 187, Transportation Research Board, Washington, D.C.
3. Zheng, Y., Sander, A. C., Rong, W., Fox, P. J., Shing, P. B., and McCartney, J. S. (2018). "Shaking table test of a half-scale geosynthetic-reinforced soil bridge abutment." *Geotechnical Testing Journal*, 41(1), 171-192.
4. Zheng, Y., McCartney, J. S., Shing, P. B., and Fox, P. J. (2019). "Physical model tests of half-scale geosynthetic reinforced soil bridge abutments. II: Dynamic loading." *Journal of Geotechnical and Geoenvironmental Engineering*, 145(11).
5. Stein, W. J., and Neuman, T. R. (2007). *Mitigation strategies for design exceptions*. FHWA-SA-07-011, U.S. DOT, Washington, D.C.
6. Duncan, J. M., Byrne, P., Wong, K. S., and Mabry, P. (1980). *Strength, stress-strain and bulk modulus parameters for finite element analysis of stresses and movements in soil masses*. Report No. UCB/GT/80-01, University of California, Berkeley, CA, USA.
7. Zheng, Y., and Fox, P.J. (2016). "Numerical investigation of geosynthetic-reinforced soil bridge abutments under static loading." *Journal of Geotechnical and Geoenvironmental Engineering*, 142(5), 04016004.
8. Zheng, Y., and Fox, P.J. (2017). "Numerical investigation of the geosynthetic reinforced soil-integrated bridge system under static loading." *Journal of Geotechnical and Geoenvironmental Engineering*, 143(6), 04017008.
9. Naesgaard, E. (2011). *A hybrid effective stress - total stress procedure for analyzing soil embankments subjected to potential liquefaction and flow*. Ph.D. Thesis. The University of British Columbia.
10. Menq, F. (2003). *Dynamic properties of sandy and gravelly soils*. Ph.D. Thesis. University of Texas, Austin.
11. Darendeli, I.S. (2001). *Development of a new family of normalized modulus reduction and material damping curves*. Ph.D. Thesis. University of Texas, Austin.
12. Caltrans. (2004). Section 5 - Retaining Walls, *Bridge Design Specifications*, August 2004.